

CFD-DEM modeling of snowdrifts on stepped flat roofs

Lei Zhao¹, Zhixiang Yu^{*1,2}, Fu Zhu¹, Xin Qi¹ and Shichun Zhao¹

¹School of Civil Engineering, Southwest Jiaotong University, Chengdu 610031, China

²Key Laboratory of High-speed Railway Engineering, Ministry of Education, Chengdu 610031, China

(Received June 1, 2016, Revised September 23, 2016, Accepted September 25, 2016)

Abstract. Snowdrift formation on roofs should be considered in snowy and windy areas to ensure the safety of buildings. Presently, the prediction of snowdrifts on roofs relies heavily on field measurements, wind tunnel tests and numerical simulations. In this paper, a new snowdrift modeling method by using CFD (Computational Fluid Dynamics) coupled with DEM (Discrete Element Method) is presented, including material parameters and particle size, collision parameters, particle numbers and input modes, boundary conditions of CFD, simulation time and inlet velocity, and coupling calculation process. Not only is the two-way coupling between wind and snow particles which includes the transient changes in snow surface topography, but also the cohesion and collision between snow particles are taken into account. The numerical method is applied to simulate the snowdrift on a typical stepped flat roof. The feasibility of using coupled CFD with DEM to study snowdrift is verified by comparing the simulation results with field measurement results on the snow depth distribution of the lower roof.

Keywords: snowdrift; CFD; DEM; snow depth distribution; flow field characteristics

1. Introduction

Snowdrift formation on roofs especially on long-span lightweight roofs is a major problem in snowy and windy areas. In recent years, with the global warming, news about structural damages due to snowdrifts were reported commonly. Majowiecki (1998) had pointed out that long-span coverings were subject to partial and global failures due to the lack of information concerning intensity and distribution on the roof surface of live loads such as wind and snow. Investigations also showed the main reasons for these accidents were big snow loads, non-uniform accumulation of snow and coupling effects of wind-snow-structure. It is of great significant to study snowdrift on roofs for the design of long-span lightweight structures resisting wind and snow.

The prediction of snowdrifts on roofs presently relies heavily on field measurements, wind tunnel tests and numerical simulations. With the development of computational mechanics especially of Computational Fluid Dynamics (CFD), an increasing number of researchers begin to study snowdrifts by numerical simulations. Meanwhile, numerical simulations have advantages on low cost, short cycle, and can be used to carry out the parametric analysis easily.

Essentially, snowdrifts include the movement of continuous phase (air) and dispersed phase (snow). Previous snowdrift modeling methods mainly base on Eulerian two-phase flow, and snow

*Corresponding author, Associate professor, E-mail: yzxzrq@home.swjtu.edu.cn

particles are regarded as a continuous phase in fact. Uematsu, Nakata *et al.* (1991) carried out the pioneering work based on CFD using the mixing length theory as the turbulence model to predict snowdrifts around a two-dimensional fence and a three-dimensional hut. This study introduced the transport equation of drifting snow density and empirical functions for erosion fluxes on the snow surface. This modeling concept had been used in most numerical simulation of snowdrift. Bang, Nielsen *et al.* (1994) described a generalized drift-flux model to simulate snowdrifts around snow fences in two dimensions and three-dimensional snow deposition around a group of houses with snow deposition expressed as surfaces. Moore (1995) developed a numerical model which can be used to predict a series of drift profiles near a particular design of building corresponding to a given time series of wind speed and direction. Sundsbø (1998) conducted a numerical study on a two-dimensional snowdrift around a porous fence in flat terrain using a one-way coupled model based on the volume of fluid (VOF) method, in which the air flow controlled the snowdrift within an Eulerian frame of air velocities. Tominaga and Mochida (1999) employed a CFD technique to the prediction of snowdrift around a nine-story apartment building using LK model. Thiis (2000) utilized a drift flux model where the fluid with snow properties was allowed to drift through a fluid with air properties to simulate snowdrift around a simple building model, and the numerical results were compared with full-scale measurements. Beyers, Sundsbø (2004) predicted transient snowdrift around a cubic structure by using the standard *k-e* turbulence model and compared the numerical results with experimental data obtained in Antarctica. Tominaga, Mochida *et al.* (2006) conducted transient CFD analysis using the revised *k-e* model for snowdrift around a cubic building model. Beyers, Sundsbø *et al.* (2008) presented a snowdrift modeling method using CFD coupled with a domain adaptation strategy to facilitate the transient changes in snow surface topography. Tominaga, Mochida *et al.* (2011) provided an overview of CFD modeling of snowdrifts around buildings and presented a new approach of a snowdrift model to predict snowdrifts around a cubic building model. Maldonado *et al.* (2012) presented a versatile three-dimensional two-phase model for simulating snow drift relocation around buildings utilizing deflection fins of various shaped and sizes. Yamagishi, Kimura *et al.* (2012) predicted the snowdrift around buildings of an Antarctic base by two-phase flow, the snow cover around a cube model was calculated by converting the volume fraction into snow depth. Zhou, Houlsby *et al.* (2015) modeled the development process of snowdrift in an open field based on the Lagrangian method, in which a splash function is adopted to research the collision of snow particles.

Previous simulations of snowdrifts simplify snow particles as a pseudo-fluid mostly, and it also has stress, pressure as well as other characteristics that only continuum possesses. The flow field characteristics are solved by adding the transport equation of snow concentration which is an empirical formula under the condition of fully development of snowdrifts to the Navier-Stokes equation of air. Snow particles are in a state of passive transportation, which is a one-way coupling, without considering the effect of snow on air. Essentially, snowdrift is a process of two-way coupling, the saltation and accumulation of snow particles are mutual interference with airflow, resulting in a non-uniform distribution. Meanwhile, the aerodynamic shape of roof may be changed due to the existence of snow, which in turn affects the movement of snowdrift. And the effect has time-varying characteristics. These limitations can be overcome by explicit calculation of the particle contact mechanics using Discrete Element Method (DEM). Coupling of DEM and CFD provides a means of momentum and energy exchange between particles and fluid, which could in principle remove the need for some of the semi-empirical approximations employed in CFD.

DEM was proposed by Cundall in 1971 (Cundall 1971), involving the Lagrangian solution for

granular flows, which explicitly calculates individual particle dynamics. With advances in computing power and numerical algorithms, DEM has been becoming widely accepted as an effective method of addressing engineering problems in granular and discontinuous materials, especially in granular flows, powder mechanics and rock mechanics.

CFD-DEM has been accepted as an advanced computational method in many research areas, such as aeolian sand movement (Zhang, Li *et al.* 2011), fluidized beds (Lu, Huang *et al.* 2014), debris flows (Zhao, Houlby *et al.* 2014) and pneumatic conveying (Brosh, Kalman *et al.* 2011). The reliability of the method has been validated in these research areas. The advantage of CFD-DEM is that it can consider the motion and force applied to every individual particle, as also as the interaction between particles and fluid. The differences between traditional Eulerian-Eulerian (E-E) model and CFD-DEM are shown in Fig. 1. In Fig. 1(a), α_{snow} refers to the volume fraction of snow in cells.

Although snowdrift belongs to the flow-induced motion with particles, as same as these above research areas, CFD-DEM has not been used in snowdrift. In this study, we propose a CFD-DEM model for simulating the snowdrift on roofs. The first part of this paper introduces the numerical simulation method, including the continuity equation and momentum equation of fluid on coupled condition, the model of snow particle, the coupling equation of fluid and particle, collision model of particles, boundary condition and framework of the coupling computation. In the latter part, the numerical method is applied to simulate the snowdrift on a stepped flat roof (Tsuchiya, Tomabechi *et al.* 2002). The feasibility of the method is verified by comparing the simulation results with the field measurement results on the snow depth distribution of the lower roof. The influence on flow field characteristics by the existence of snow on roofs is also discussed.

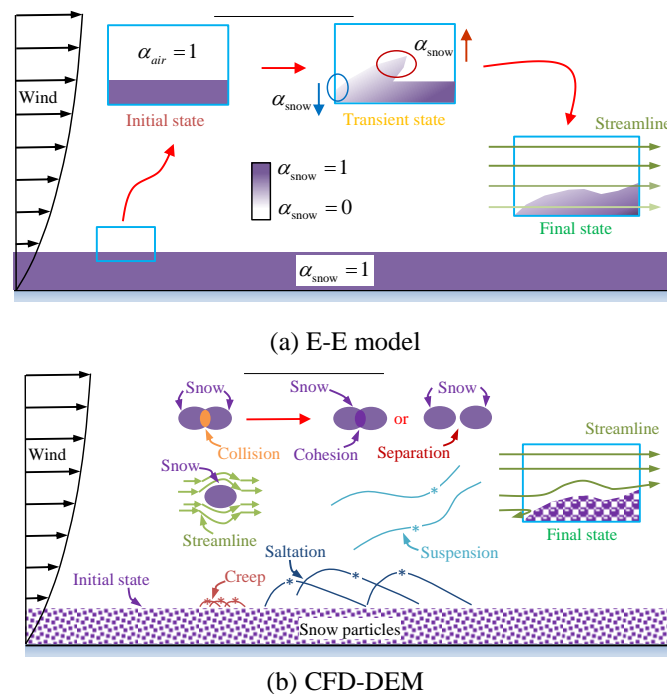


Fig. 1 Differences between E-E model and CFD-DEM

2. Mathematical models

2.1 Equations governing the air phase

Energy transfer is ignored, meaning that only mass and momentum need to be conserved. The continuity equation for the air flow is given by Eq. (1)

$$\frac{\partial}{\partial t}(\alpha_F \rho_F) + \nabla \cdot (\alpha_F \rho_F \mathbf{v}_F) = \frac{\partial}{\partial t}(m_p) \quad (1)$$

where the subscript F refers to air and p refers to snow particle, α is the volume fraction, ρ is the density, \mathbf{v} is the velocity and m is the mass.

The rate of change of the snow mass in any grid cell is given by Eq. (2)

$$\frac{\partial m_p}{\partial t}(t) = m_p(t) - m_p(t - \tau) \quad (2)$$

where τ is the time-step of CFD.

A similar equation exists for the conservation of momentum is given by Eq. (3)

$$\frac{\partial}{\partial t}(\alpha_F \rho_F \mathbf{v}_F) + \nabla \cdot (\alpha_F \rho_F \mathbf{v}_F \mathbf{v}_F) = -\alpha_F \nabla p + \nabla \cdot \boldsymbol{\tau}_F + \alpha_F \rho_F \mathbf{g} - \mathbf{f}_{drag} \quad (3)$$

where $\boldsymbol{\tau}_F$ is the stress tensor and p is the pressure shared by air and snow, \mathbf{g} is the gravitational acceleration and \mathbf{f}_{drag} is the average drag force.

$\boldsymbol{\tau}_F$ and \mathbf{f}_{drag} are calculated by Eqs. (4) and (5), respectively

$$\boldsymbol{\tau}_F = -\frac{2}{3}(\mu_{eff} \nabla \cdot \mathbf{v}_F) \mathbf{I} + \mu_{eff} [\nabla \cdot \mathbf{v}_F + (\nabla \cdot \mathbf{v}_F)^T] \quad (4)$$

$$\mathbf{f}_{drag} = \frac{1}{\Delta V} \sum_{i=1}^{n_p} \mathbf{F}_{drag,i} \quad (5)$$

where μ_{eff} is the effective viscosity of air, \mathbf{I} is the unit tensor and n_p is the number of snow particles

The drag force of particle i named $\mathbf{f}_{drag,i}$ is given by Eq. (6)

$$\mathbf{f}_{drag,i} = 0.5 C_D \rho_F A_p (\mathbf{v}_F - \mathbf{v}_p) |\mathbf{v}_F - \mathbf{v}_p| \quad (6)$$

where A_p is the projected area of the particle and C_D is drag coefficient depending on the Reynolds number Re according to Eqs. (7) and (8).

$$Re = \frac{\alpha_F \rho_F d_p |\mathbf{v}_F - \mathbf{v}_p|}{\mu_F} \quad (7)$$

$$C_D = \begin{cases} 24 / Re & Re \leq 0.5 \\ 24(1.0 + 0.15 Re^{0.687}) / Re & 0.5 < Re \leq 1000 \\ 0.44 & Re > 1000 \end{cases} \quad (8)$$

where d_p denotes the diameter of the particle, μ_F denotes the viscosity coefficient of the air.

2.2 Equations governing the particle

The translation and rotation motion equations of snow particles are governed by Eqs. (9) and (10), respectively, which considering the gravity, the collision and the drag force.

$$m_p \frac{d\mathbf{v}_{p,i}}{dt} = m_p \mathbf{g} + \mathbf{F}_{\text{drag},i} + \sum_{j=1}^{n_c} (\mathbf{F}_{nij} + \mathbf{F}_{tij}) \quad (9)$$

$$I_p \frac{d\boldsymbol{\omega}_i}{dt} = \sum_{j=1}^{n_c} \mathbf{T}_{ij} \quad (10)$$

where m_p , $\mathbf{v}_{p,i}$ and $\boldsymbol{\omega}_p$ are the mass, the linear velocity and the angular velocity of particle i , respectively; \mathbf{F}_{nij} , \mathbf{F}_{tij} and \mathbf{T}_{ij} are the normal contact force, the tangential contact force and the contact moment between particle i and particle j , respectively; I_p is the moment of inertia of particle, n_c is the total number of particles that impact particle i at the same time. \mathbf{T}_{ij} and I_p are given by Eqs. (11) and (12), respectively

$$\mathbf{T}_{ij} = \mathbf{D}_i \times (\mathbf{F}_{nij} + \mathbf{F}_{tij}) \quad (11)$$

$$I_p = \frac{1}{10} m_p d_p^2 \quad (12)$$

where \mathbf{D}_i is the distance vector between the center of mass of particle i to the contact point.

2.3 Equations governing the coupling

Interaction between snow particles and air is simulated by volume fraction denoted as α when using coupled CFD with DEM to study snowdrift. The volume fraction of snow particles denoted as α_p and the volume fraction of air denoted as α_f in mesh cell are given by Eqs. (13) and (14), respectively

$$\alpha_p = \sum_{k=1}^{n_p} V_{pk} / \Delta V \quad (13)$$

$$\alpha_f = 1 - \alpha_p \quad (14)$$

where n_p is the total number of particles in the mesh cell, V_{pk} and ΔV are the volume of particle k and the mesh cell, respectively.

2.4 Particle collision model

According to the linear spring-damper contact model (Crowe, Sommerfeld *et al.* 1998), the normal contact between snow particles is simulated by spring and damper, the tangential contact between snow particles is simulated by spring, damper and slider, as shown in Fig. 2. Contact force is calculated according to the normal amount of overlap and the tangential displacement between snow particles, where surface deformation of snow particles and contact force loading history are ignored.

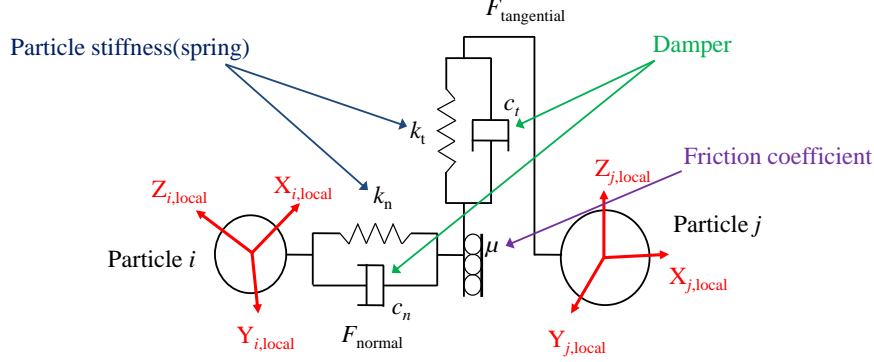


Fig. 2 Particle collision model

\mathbf{F}_{nij} denoting the normal contact force is given by Eq. (15)

$$\mathbf{F}_{nij} = (-k_n \alpha^{1.5} - c_n \mathbf{G} \mathbf{n}) \mathbf{n} \quad (15)$$

where k_n is the normal spring coefficient and c_n is the normal damping coefficient, α is the normal amount of overlap and \mathbf{G} is the relative velocity between particle i and particle j , given by Eq. (16) and \mathbf{n} is the unit normal vector from the center of particle i to the centre of particle j .

$$\mathbf{G} = \mathbf{v}_i - \mathbf{v}_j \quad (16)$$

\mathbf{F}_{tij} denotes the tangential contact force is given by Eq. (17)

$$\mathbf{F}_{tij} = \begin{cases} -k_t \boldsymbol{\delta} - c_t \mathbf{G}_{ct} & |\mathbf{F}_{tij}| \leq \mu |\mathbf{F}_{nij}| \\ -\mu |\mathbf{F}_{nij}| \mathbf{t} & |\mathbf{F}_{tij}| > \mu |\mathbf{F}_{nij}| \end{cases} \quad (17)$$

where k_t is the tangential spring coefficient and c_t is the tangential damping coefficient, $\boldsymbol{\delta}$ is the tangential displacement of the contact point, μ is the friction coefficient between snow particles, \mathbf{G}_{ct} is the slip velocity of the contact point, given by Eq. (18) and \mathbf{t} is the unit tangential vector.

$$\mathbf{G}_{ct} = \mathbf{G} - (\mathbf{G} \mathbf{n}) \mathbf{n} + d_i \boldsymbol{\Omega}_i \times \mathbf{n} + d_j \boldsymbol{\Omega}_j \times \mathbf{n} \quad (18)$$

where d_i and d_j , $\boldsymbol{\Omega}_i$ and $\boldsymbol{\Omega}_j$ are the diameter and the angular velocity of particle i and particle j , \mathbf{n} is the unit normal vector from the center of particle i to the center of particle j .

The stiffness k_n can be given by Eq. (19) using the Hertzian contact theory (Johnson 1985)

$$k_n = \frac{4}{3} \left(\frac{1-\nu_i^2}{E_i} + \frac{1-\nu_j^2}{E_j} \right)^{-1} \left(\frac{d_i + d_j}{d_i d_j} \right)^{-1/2} \quad (19)$$

where ν_i and ν_j , E_i and E_j , d_i and d_j are the Poisson ratio, Young's modulus and the diameter of particle i and particle j respectively.

The stiffness k_t can be given by Eq. (20) using the Mindlin's theory (Mindlin 1949)

$$k_t = 8\delta^{1/2} \left(\frac{1-\nu_i^2}{G_i} + \frac{1-\nu_j^2}{G_j} \right)^{-1} \left(\frac{d_i + d_j}{d_i d_j} \right)^{-1/2} \quad (20)$$

where α is the normal amount of overlap, ν_i and ν_j , G_i and G_j , d_i and d_j are the Poisson ratio, shear modulus and the diameter of particle i and particle j respectively.

The normal damping coefficient denoted c_n and the tangential damping coefficient denoted c_t can be given by Eqs. (21) and (22) according to Cundall and Strack (1979)

$$c_n = 2\sqrt{mk_n} \quad (21)$$

$$c_t = 2\sqrt{mk_t} \quad (22)$$

where m is the mass, k_n and k_t are the normal spring coefficient and the tangential spring coefficient respectively.

Cohesions are taken into account by adding normal cohesion force to the above spring-damper contact model, and the normal cohesion force denoted as F_c is given by Eq. (23)

$$F_c = KA \quad (23)$$

where K is the energy density and A is the contact area.

3. Simulation methodology

Study on snowdrifts in this paper mainly refer to the case that the roof is covered by an initial uniform snow with a certain depth without other particles input, under wind load the movement of snow particles in the form of creep, saltation and suspension are occurred, forming a non-uniform distribution until a new stable shape under the interaction between wind and snow particles.

3.1 Material parameters and particle size

The snow density is variable relating to its falling and sedimentation condition closely. The scholars from the former Soviet Union (Машгиз 1967) believe that this kind of density ranges from 10 kg/m^3 to 800 kg/m^3 , equivalent to the density between air and ice. The size of snow particles changes a lot at the same time, but the diameter is usually less than 4 mm.

Snow particles are simulated by the classical spherical model in DEM, and the complex physical phenomena of snow particles such as sublimation and thawing are ignored. The size of snow particles is simulated as Gaussian distribution, the average value is 3 mm and the standard deviation is 0.05 according to measured results. The density of snow particles are set to 30 kg/m^3 based on the principles of equivalent weight with the actually measured value. Before the coupling of CFD and DEM, snow on the roof with a certain depth should be initialized in DEM to accelerate the computation.

The modulus of elasticity of snow particles is given by Eq. (24) according to the result researched by Scapozza and Bartelt (2003) The Poisson's ratio of snow particles is set to 0.25.

$$E = 0.10 \exp(0.015\rho + 0.06|\theta|) \quad (24)$$

where ρ is the density, the unit is kg/m^3 ; θ is the temperature set as -10°C in this paper.

Material of walls is set to concrete, related parameters are needless to describe here.

3.2 Collision parameters

Parameters for collision models are shown in Table 1. Parameters are estimated according to massive tests and parametric analysis due to they have not been researched in previous papers.

3.3 Particle numbers and input modes

The number of particles mainly depends on the total volume of snow on the roof and the size of snow particles, when the gaps between particles are ignored, the number of particles are given by Eq. (25)

$$n_c = \frac{V_s}{V_p} \quad (25)$$

where n_c is the total number of particles in simulation; V_s is the total volume of snow on the roof in nature; V_p is the average volume of snow particles in simulation.

Three different input modes can be adopted to simulate snow in DEM and couple with CFD, as shown in Fig. 3. Mode 1 and mode 3 only contain either initial snow or snow inlet during the simulation respectively. Both initial snow and snow inlet are considered in mode 2. However, the cost of computing time will be very high when snow inlet mode is adopted in accordance with the actual snow. When increasing the particle number input per unit time, the driven energy obtained from the flow field by each particle will be weakened, resulting in an incorrect stable accumulation form. Therefore, mode 1 and mode 2 may be more reasonable options, and it will be proved later.

3.4 Boundary conditions of CFD

Boundary conditions are summarized in Table 2. Inlet is velocity-inlet and power law is used to represent the variation of wind speed with height, the ground roughness exponent denoted as α is 0.16 according to the suggestion by Davenport (1965), outlet is outflow, Realizable k - ϵ model combined with enhanced wall function are used to turbulence closure. Building walls and ground are wall condition, upper face and side are symmetry condition.

Table 1 Collision parameters

	Snow to Snow	Snow to Concrete
Coefficient of Restitution	0.01	0.01
Coefficient of Static Friction	0.05~0.2	0.3
Coefficient of Rolling Friction	0.05	0.1
Energy Density ($\text{J}\cdot\text{m}^{-3}$)	11000	11000

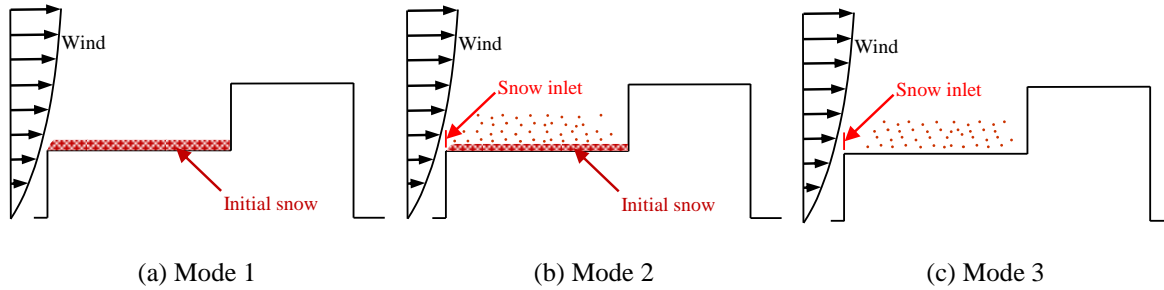


Fig. 3 Three different input modes

Table 2 Boundary conditions of CFD

	Type	Parameters
Inlet	velocity-inlet	$u = v_b \times \left(\frac{z}{z_b}\right)^\alpha$
		$I_u = \begin{cases} 0.23 & z < 5m \\ 0.1 \times \left(\frac{z}{350}\right)^{-0.21} & 5m \leq z \leq 350m \end{cases}$
Turbulence	Realizable k - ε	$k = \frac{3}{2}(uI_u)^2$, $\varepsilon = C_\varepsilon^{3/4} \frac{k^{3/2}}{L}$, $C_\varepsilon = 0.09$, $L = 100\left(\frac{z}{30}\right)^{0.5}$
Outlet	outflow	$\partial\psi / \partial n = 0$, Ψ denotes all flow variables except pressure
Building walls	wall	$u, v, w = 0$
Ground	wall	$u, v, w = 0$
Upper face and side	symmetry	$\partial u / \partial n = 0$

3.5 Simulation time and inlet velocity

The simulation time and inlet velocity are determined by the following 3 basic principles:

- (1) The principle of the truncation of simulation time is that the accumulation form reaches a stable state. The criterion of stable state is that the normalized depth (s/s_{\max}) distribution has to basically remain unchanged.
- (2) The principle of simulation time related to physical time is that the number of snow particles located on the roof has to be basically the same.

- (3) The principle of wind speed compensation is that the average particle kinetic energy in each model of different particle transportation mode has to be basically the same.

3.5.1 Equivalent conversion of simulation time with physical time

Assuming that the number of particles on the roof in simulation and in nature are equal

$$n_C = n_N \quad (26)$$

where n_N is the total number of particles on the roof in nature.

Physical time denoted as T_N is given by Eq. (27)

$$T_N = \frac{n_N}{n_{iN}} \quad (27)$$

where n_{iN} is the number of particles located on the roof per unit time in nature.

Simulation time denoted as T_C is given by Eq. (28)

$$T_C = \frac{n_C}{n_{iC}} \quad (28)$$

where n_{iC} is the number of particles inlet in the computational domain per unit time in simulation.

The ratio of particle inlet in nature and in simulation is denoted as λ_n

$$\lambda_n = \frac{n_{iN}}{n_{iC}} \quad (29)$$

In consideration of some particles may run out of the computational domain in the form of suspension in simulation, an inequality (30) is required.

$$T_C \geq \lambda_n T_N \quad (30)$$

3.5.2 Equivalent conversion of wind speed compensation

The kinetic energy of a single particle in nature and in simulation are denoted as E_{pi-N} and E_{pi-C} respectively, only if $E_{pi-N} \approx E_{pi-C}$, driven energy obtained by each particle in simulation may approximate that in nature. The total kinetic energy of particles in nature and in simulation denoted as E_N and E_C respectively can be calculated by Eqs. (31) and (32).

$$E_N = \sum E_{pi-N} = \sum \frac{1}{2} m_{iN} v_{iN}^2 \quad (31)$$

$$E_C = \sum E_{pi-C} = \sum \frac{1}{2} m_{iC} v_{iC}^2 \quad (32)$$

where m_{iN} and m_{iC} , v_{iN} and v_{iC} are the mass and velocity of each particle in nature and in simulation respectively.

The ratio of particle velocity in simulation and in nature is denoted as γ_v

$$\gamma_v = \frac{v_{iC}}{v_{iN}} \quad (33)$$

In order to ensure the stable accumulation form is consistent and average particle kinetic energy is approximately equal, v_{iC} should be modified according to E_{pi-C} and n_{iC} , given by Equation (34).

$$v_{iC} = f(E_{pi-C}, n_{iC}) \quad (34)$$

Furthermore, the relationship can be obtained by numerical simulations.

3.6 Coupling calculation process

The calculation processes of snowdrifts using CFD coupled with DEM are as follows:

(1) Initialize the problem and cover the roof with snow particles in DEM as the initial model, mainly d_p denoting the diameter of snow particle, ρ_p denoting the density of snow particle and collision parameters included;

(2) Set the boundary condition and turbulence model in CFD, mainly \mathbf{u} denoting the inlet velocity, k denoting the turbulence kinetic energy and ε denoting the turbulent dissipation included;

(3) Iterate to convergence including the continuity equation (Eq. (1)) and the momentum equation (Eq. (3)) in CFD;

(4) Calculate α_F denoting the volume fraction of air (Eq. (13)), α_p denoting the volume fraction of snow particles (Eq. (14)) and F_{drag} denoting the drag forces (Eq. (6))

(5) Calculate the translation and rotation of snow particles under the comprehensive effect of gravity, F_{nij} denoting the normal contact force, F_{tij} denoting the tangential contact force and F_{drag} denoting the drag forces in DEM (Eqs. (9) and (11))

(6) Update the acceleration, velocity and position of snow particles;

(7) Calculate the rate of change of the snow mass (Eq. (2)) and update the continuity equation (Eq. (1)) and the momentum equation (Eq. (3)) in CFD;

(8) Start calculation of the next time-step until the simulation time.

Fig. 4 shows the calculation processes of snowdrifts using CFD coupled with DEM.

4. Numerical simulation

4.1 Typical snowdrift formation

Snowdrift formation represented by Fig. 5 is a typical formation. It behaves as that serious erosion and reaccumulation of snow exist in these areas where influenced by vortex on the windward side, vortex on the leeward side and separation on the roof. Judging from the coupling

effect of air and snow particles, when the force on snow particle by air is bigger than the weight, cohesion and friction of the snow particle, it may move from the larger wind area to the smaller wind area on the form of creep, saltation and suspension, resulting in erosion in vortex areas, as shown in Fig. 6. The changes of snowdrift formation will change its surrounding flow field at the same time, such as decelerating the air flow. Snow particles may reaccumulate and bond, forming a stable accumulation form when the velocity of airflow is lower than a critical value, resulting in a relatively fixed model of snowdrift formation, and it is the stable equilibrium state by the two-way coupling of wind and snow particles actually. Snowdrift formation showed in Fig. 6 will not disappear with the changing of building shape as long as the air flow is obstructed by bluff body, forming the typical airflow movement such as vortex and separation. The difference is only on the degree of erosion and the height of snow accumulation, and they mainly depend on the strength of the vortex and the characteristic of snow particles, such as size, density and viscosity.

CFD-DEM method will be applied next to simulate the snowdrift on a stepped flat roof.

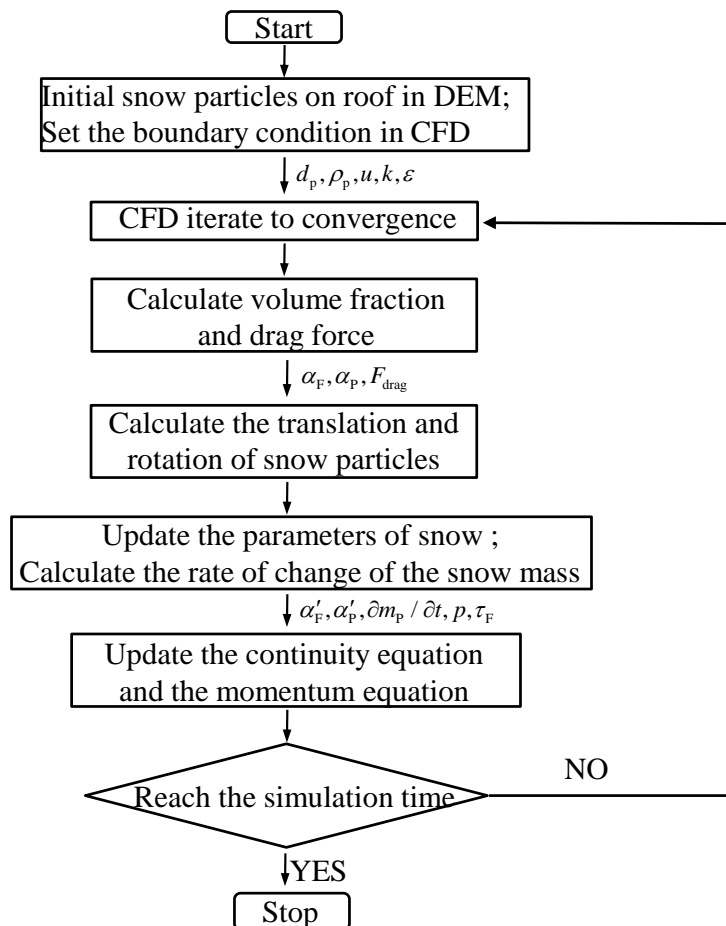


Fig. 4 Coupling calculation process

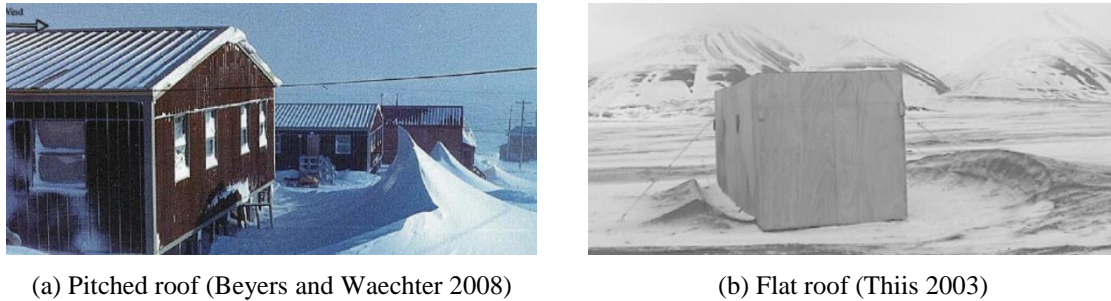


Fig. 5 Typical snowdrift formation

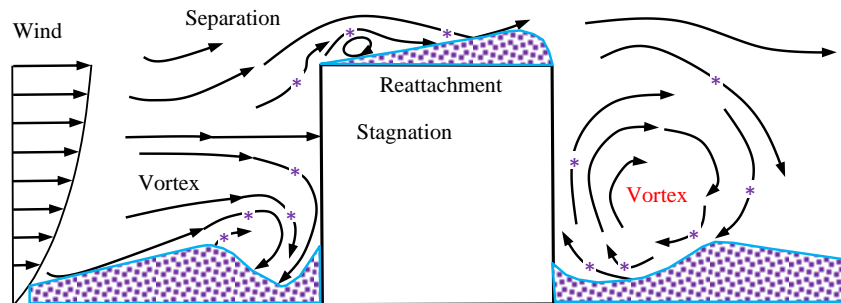


Fig. 6 Flow characteristic and snowdrift formation

4.2 Model introduction

In fact, snowdrift is a 3D movement in nature, and the accumulation mainly depends on the characteristics of flow field. Past studies on the flow characteristics around bluff bodies have shown that it is very successful to obtain the flowing characteristics on typical section of bluff bodies using a 2D model when some certain conditions are satisfied, especially those numerical simulation results based on RANS model are basically identical with 3D test results (Murakami 2000).

Stepped roof is one of the common roof forms. Under snow drifting, snows on the lower roof is more serious due to its flow characteristic. The preceding method is adopted here to simulate the snowdrift on a typical stepped flat roof model (Fig. 7(a)) which had been used by Tsuchiya (2002) in field measurement tests. The model whose lower roof on the windward side is used here. The software of CFD is Fluent 15.0 and the software of DEM is EDEM 2.7.

In view of that the model is symmetry perpendicular to the direction of flow and the width is larger, so flow field section can be considered to have average features except these corners, especially in symmetric section, it is consistent with the discussions about simplification from 3D to 2D (Emil and Robert 1986). Meanwhile, calculational consumption will be greatly reduced by simplifying 3D model to 2D model. So a 2D model was constructed ($H=0.9$ m), and the length of the computational domain was 31m, the height was 10m, the width was 0.1m dividing in 2 layers whose thickness was 0.05 m. Structural grid partition was adopted (Fig. 7(b)), and the minimum mesh size was 0.01 m in near wall region.

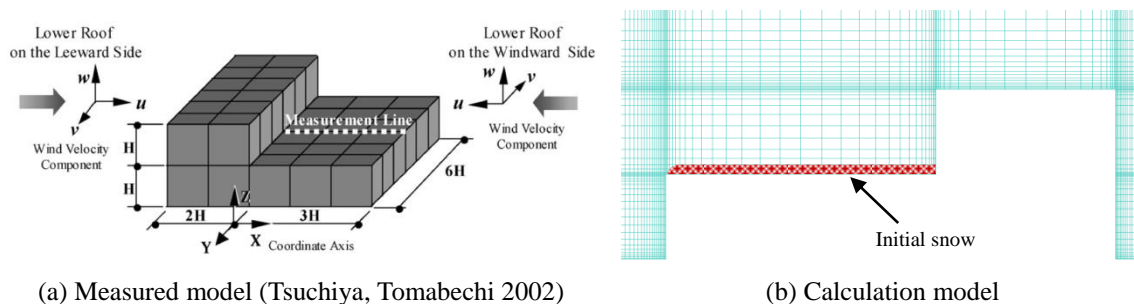


Fig. 7 Diagram of calculation model

Before coupling calculation, initial snow with a certain depth is generated using the preceding parameters on the lower roof (Fig. 6(b)). Time step of DEM for snow particle is closely related to its density and size, and according to user guide (EDEM 2.7 User Guide 2015), when the time step set as 30%~70% of Rayleigh time step, calculated results will be reliable. CFD typically uses a time step of orders of 10–100 greater than DEM. The simulation time is determined according to the total particle numbers and particle generation rate.

4.3 Coupling motion process

Streamlines around the model and snow depth distribution of the lower roof at different time are shown in Fig. 8. Separation and vortex occur at the frontal edge of the lower roof, which lead to the movement of suspensions with the oblique upward direction and creeps with the direction opposed to the main wind direction. Movements of snow particles at the middle and later of the lower roof are saltation and creep mainly, and a part of snow particles are accumulated at the end of the lower roof after impacting the wall of the higher roof. Meanwhile, erosion is very serious due to the influence of vortex at the end of the lower roof, resulting in a non-uniform accumulation. The snow depth distribution of the lower roof is basically stable after 1.0s, and the steady state performs that snow particles at the front and middle of the lower roof creep to the frontal edge due to backflow, and suspensions occur when snow particles reach the frontal edge due to separation of flow field.

4.4 Snow depth distribution

Fig. 9 shows the snow depth distribution of the lower roof at 1.0s by numerical simulation using CFD coupled with DEM, compared with that in field observations (Tsuchiya, Tomabechi *et al.* 2002), wind tunnel test (Wang, Liao *et al.* 2014) and in Japanese code (Architectural Institute of Japan 2006). The vertical axis denotes the snow depth ratio (s/S_d) obtained by dividing the snow depth (s) on the lower roof with the depth of ground snow (S_d). But for the simulation and wind tunnel test results, S_d denotes the initial snow depth on the lower roof. Due to the snow depth distribution in Japanese code is get from an actual photo, the distribution curve is adjusted by the same proportion to ensure the maximum of s/S_d is consistent with numerical simulation. It shows that the snow depth distribution in field measurements, numerical simulation, wind tunnel test and

Japanese code are similar to each other. s/S_d gradually increases from the frontal edge to the end of the lower roof, but at the end of the lower roof, erosion is very obvious due to the existence of vortex. Simulation result is in good agreement with Japanese code at $x/H < 1.0$ and $x/H > 2.5$, but in good agreement with field measurements and wind tunnel test at $x/H = 1.0 \sim 2.5$.

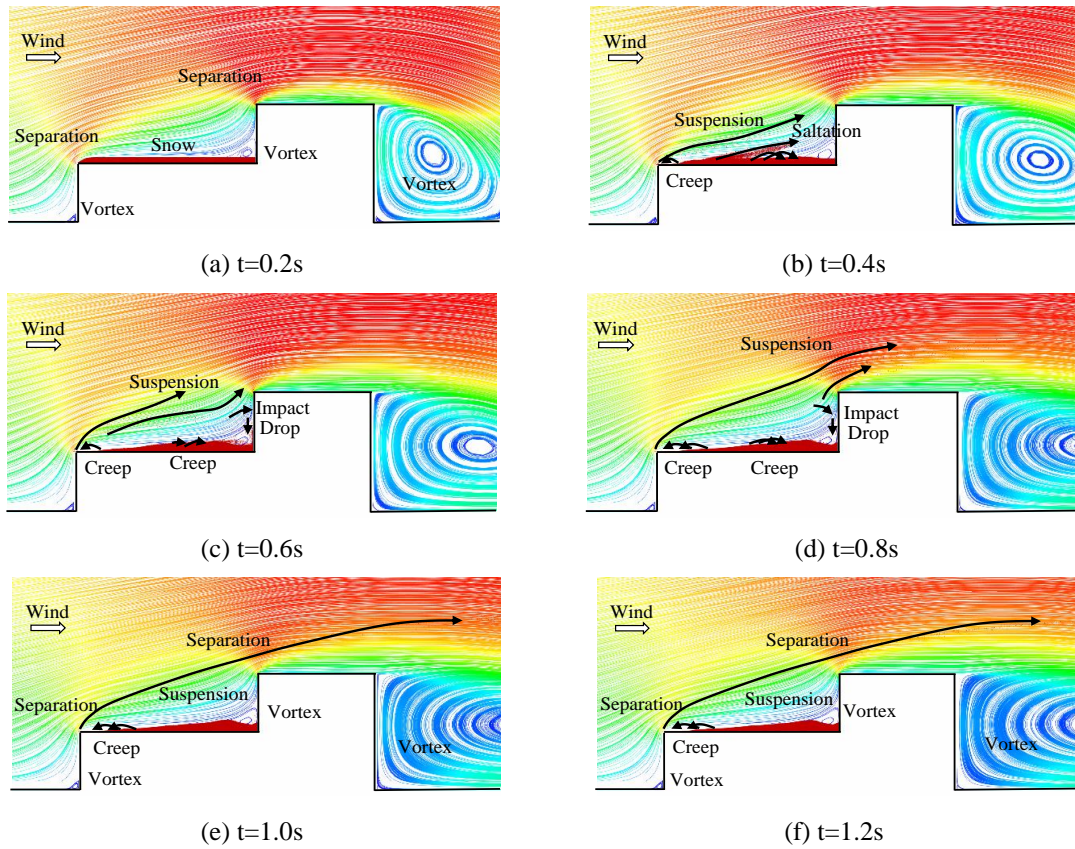


Fig. 8 Streamlines and snow depth distribution

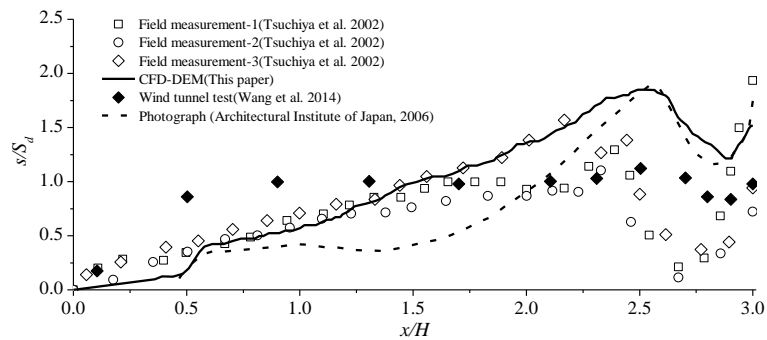


Fig. 9 Snow depth distribution on the lower roof

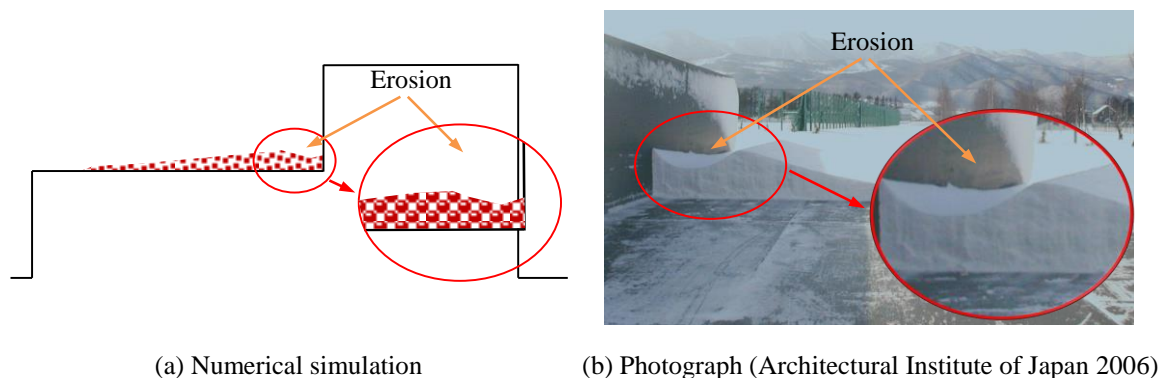


Fig. 10 Snow distribution at the end of the lower roof

Although the simulation result is similar to the existing results, there are some small differences in the snowdrift peak location and value, as well in the snow depth distribution at the frontal edge of the lower roof. The reasons for these differences maybe lies mainly in the differences of wind velocity and wind directions, the location for the model and the properties of snow particles. In addition, the $k-\varepsilon$ turbulence model used in numerical simulation may be also a main reason due to its limitation, which is well known for that the turbulence model may overestimate the turbulent kinetic energy at the frontal edge and underestimate the turbulent kinetic energy at the end of the roof. A further investigation should be carried out to evaluate different turbulence models which may improve the predicted snowdrift formation and reduce the effects of the known deficiencies of the $k-\varepsilon$ turbulence model.

Fig. 10 shows photos of the snow distribution at the end of the lower roof by numerical simulation compared with that in Japanese code (Architectural Institute of Japan 2006). The form of snowdrifts accumulations are similar to each other, characterized by an obvious pit due to erosion. Snows on the roof finally form a new stable shape under the interaction between wind and snow.

4.5 Prediction of physical time

Aiming at the prediction of physical time, 4 cases (Table 3) have been designed to simulate the snowdrift under snowstorm. According to the regulations of the meteorological evaluation of China, case 1 with 100 mm initial depth corresponds to the actual snowstorm of 24 hours (<http://www.cma.gov.cn>). Obviously, if the simulation according to the actual physical time will consume too much computing time, therefore, increasing the number of particles transport per unit time and improving the inlet velocity have been adopted according to section 3.4, an approximate relationship between simulation and physical time has been built.

Accumulation forms at a certain time of each case are as shown in Fig. 11. Although the particle inlet modes are different between case 1 and case 2, the final stable accumulation forms are basically identical, it proves that the change of particle input mode is effective.

However, due to the accelerated calculation is adopted, the number of particle transport per unit time in case 1 and case 2 are much larger than that in natural snowfall process. Therefore, under

the condition of the same inlet velocity, the wind induced effect on a single particle in these accelerated cases may be lower than that in natural snowfall process, affecting the prediction of accumulation form. In order to demonstrate the effect of the factor, case 3 and case 4 have been designed, these characteristics are given below:

- (1) There are no initial snow on the lower roof and particles are inputted at the front of the lower roof.
- (2) Ensure that the average particle kinetic energies are basically same by adjusting the inlet velocity.

The results show that the stable accumulation forms of these cases are basically identical, but the accelerating effects of case 1~3 are very significant. It indicates that the efficiency of snowdrift simulation can be greatly increased by improving the number of particles transport per unit time and compensating the wind speed.

Table 3 Models with different particles transport per unit time

	h_0 (m)	n_0	n_t	n_c	d (mm)	v_b (m/s)	t_0 (s)	T_N (h)
Case 1	0.1	126920	0	124720	$d \sim N(3, 0.05^2)$	24	1	24
Case 2	0.05	63562	10000	75658	$d \sim N(3, 0.05^2)$	15	1.5	14
Case 3	0	0	5000	68543	$d \sim N(3, 0.05^2)$	24	-	13
Case 4	0	0	500	43353	$d \sim N(3, 0.05^2)$	12	-	8

* h_0 : Initial depth; n_0 : Initial number of particles; n_t : Particle generation rate; d : Particle size; t_0 : Stable time

Table 4 Models with different particle numbers

	h_0 (m)	n_0	d (mm)	v_b (m/s)
Case 1	0.1	126920	$d \sim N(3, 0.05^2)$	24
Case 2	0.075	95311	$d \sim N(3, 0.05^2)$	24
Case 3	0.05	63562	$d \sim N(3, 0.05^2)$	24

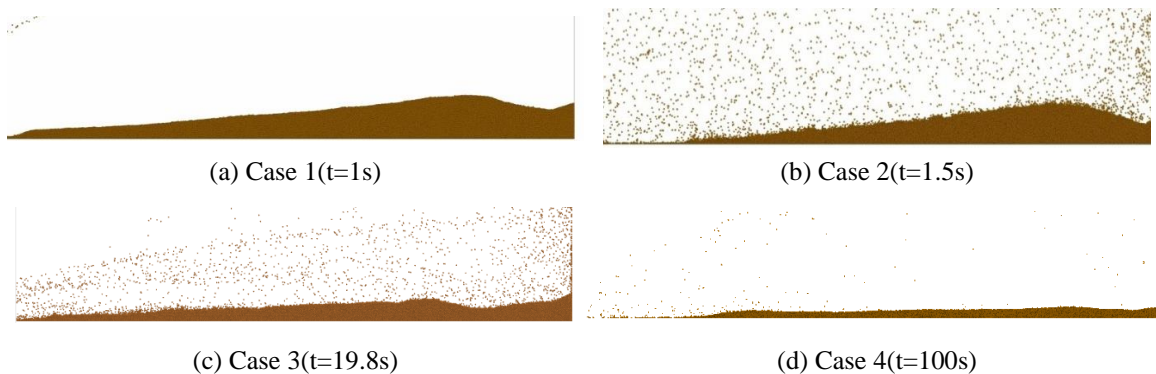


Fig. 11 Accumulation form of each case

* Accumulation form of case 3 and case 4 are not stable, but similar to case 1 and case 2

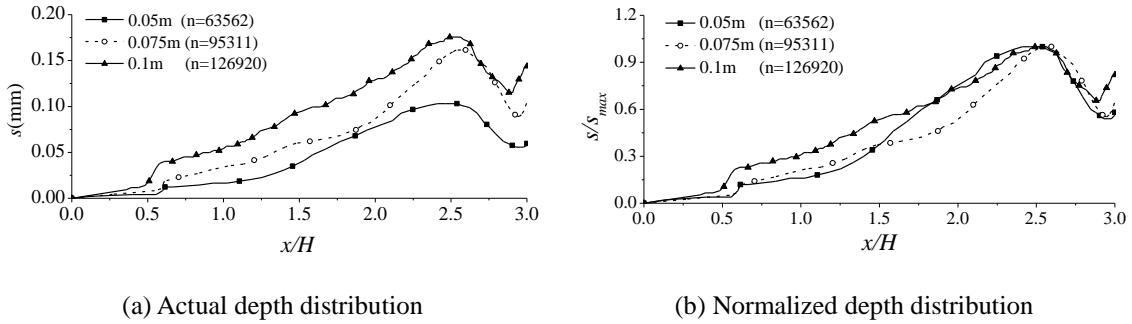


Fig. 12 Effect of particle numbers

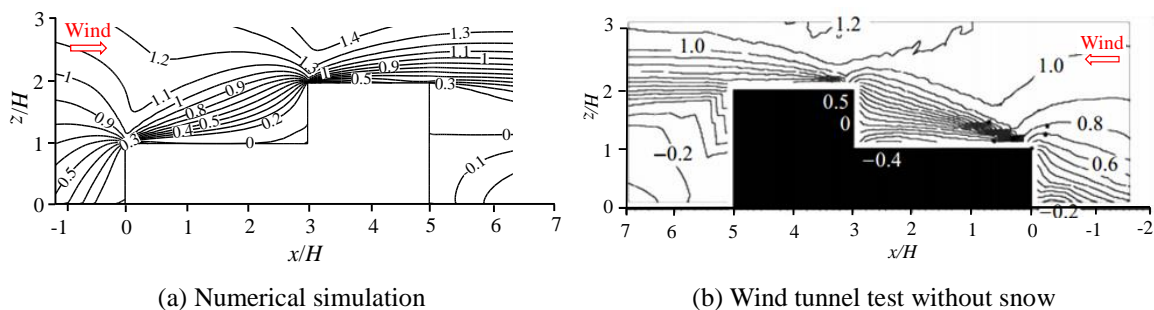
4.6 Effect of particle numbers

In order to research the effect of particle numbers, 3 cases with different numbers (Table 4) were simulated. The final stable accumulation forms are shown in Fig. 12. The results show that:

- (1) The change of particle numbers mainly affects the relative depth of accumulations.
- (2) Although particle numbers are different, the stable accumulation forms are basically identical. Tiny difference is that with the increase of particle numbers, the gradient of accumulations becomes slower gradually.

4.7 Influence on flow field characteristics

Fig. 13 shows the contour of the dimensionless horizontal wind velocity (u/U_0), where U_0 is the horizontal wind velocity at the lower roof height. Fig. 13(a) shows the result of numerical simulation after snows on the lower roof is stable; Fig. 13(b) shows the result of wind tunnel test without snow by Tsuchiya (Tsuchiya, Tomabechi *et al.* 2002). The contour of u/U_0 in numerical simulation results (Fig. 13(a)) is similar to that in wind tunnel test results (Fig. 13(b)) in these areas of above the higher roof ($x/H=3\sim 5$) and behind the model ($x/H>5$), where the snow particles affect it much less, and the consistency also can prove the accuracy of the numerical simulation to some extent.

Fig. 13 Contours of the dimensionless horizontal wind velocity u/U_0

However, near the lower roof where the aerodynamic shape is signally affected by the existence of snow. There are big difference between numerical simulation results (Fig. 13(a)) with wind tunnel test results (Fig. 13(b)) in the contour of u/U_0 , owing to that the change of aerodynamic shape disturbs and weakens the vortex obviously, especially in the middle of the lower roof ($x/H=1\sim 2.5$), $u/U_0 < 0$ means that there is no vortex. But in the wind tunnel test results (Fig. 13(b)), the minimum value of u/U_0 is -0.4 at the same area, meaning that the vortex is fairly significant.

5 Conclusions

1) A two-way coupling method for snowdrift modeling by using CFD coupled with DEM has been established firstly. The governing equations and the key parameters have been presented, including collision model, material parameters and boundary conditions.

2) CFD-DEM modeling method has been used to simulate the snowdrifts of a typical flat stepped roof in 2D, snow depth distribution of the lower roof by numerical simulation is similar to that in field measurements and wind tunnel test, so the validity of the method has been verified.

3) The change of particle numbers mainly affects the relative depth of accumulations, and with the increase of particle numbers, the gradient of accumulations becomes slower gradually.

4) The change of aerodynamic shape due to the existence of snow may disturb and weaken the vortex obviously, resulting in a significant effect on the wind loads of the roof. A further research is deserved to be carried out to evaluate the effect of snowdrift on the wind loads of roofs.

Acknowledgements

The work of this study was supported by the National Natural Science Foundation of China under Grant No. 51378428 and No.51408500, the foundation of State Key Laboratory of Geohazard Prevention and Geoenvironment Protection under Grant No. SKLGP2016K013.

References

- Architectural Institute of Japan (2006), "Commentary on Recommendations for Loads on Buildings-Chapter 5 snow loads", Tokyo, Japan.
- Bang, B., Nielsen, A. and Sundsbø, P.A. and Wiik, T. (1994), "Computer simulation of wind speed, wind pressure and snow accumulation around buildings (SNOW-SIM)", *Energ. Buildings*, **21**(3), 235-243.
- Beyers, J.H.M., Sundsbø, P.A. and Harms, T.M. (2004), "Numerical simulation of three-dimensional transient snow drifting around a cube", *J. Wind Eng. Ind. Aerod.*, **92**, 725-747.
- Beyers, M. and Waechter, B. (2008), "Modeling transient snowdrift development around complex three dimensional structures", *J. Wind Eng. Ind. Aerod.*, **96**, 1603-1615.
- Brosh, T., Kalman, H. and Levy, A. (2011), "Dem simulation of particle attrition in dilute-phase pneumatic conveying", *Granular Matter*, **13**(2), 175-181.
- China Meteorological Administration (2009) <http://www.cma.gov.cn>
- Crowe, C.T., Sommerfeld, M. and Tsuji, Y. (1998), *Multiphase Flows With Droplets and Particles*, CRC Press, Boca Raton, Florida, USA.
- Cundall, P.A. (1971), *A Computer Model for Simulating Progressive, Large-Scale Movements in Block Rock Systems*, Symposium of International Society of Rock Mechanics, Vol.1(ii-b), 11-8.
- Cundall, P.A. and Strack, O.D.L. (1979), "A discrete numerical model for granular assemblies", *Géotechnique*, **29**(1), 47-65.
- Davenport, A.G. (1965), "The relationship of wind structure to wind loading", *Proceedings of the*

- Symposium on Wind Effect on Building and Structure*, London, Britain.
- DEM Solutions (2015), "EDEM 2.2 User Guide".
- Emil, S. and Robert, H.S. (1986), *Wind effects on structures: An introduction to wind engineering*, 2nd Ed., Wiley-Interscience, New York, USA.
- Johnson, K.L. (1985), "Contact Mechanics", Cambridge Univ. Press, NY.
- Lu, Y., Huang, J. and Zheng, P. (2014), "Fluid hydrodynamic characteristics in supercritical water fluidized bed: a dem simulation study", *Chem. Eng. Sci.*, **117**(1), 283-292.
- Majowiecki, M. (1998), "Snow and wind experimental analysis in the design of long-span sub-horizontal structures", *J. Wind Eng. Ind. Aerod.*, **74-76**, 795-807.
- Maldonado, E. and Roth, M.W. (2012), "Direct two-phase numerical simulation of snowdrifts external to building walls and remediation with deflection fins", *J. Appl. Fluid Mech.*, **5**(3), 71-78.
- Mindlin, R.D. (1949), "Compliance of elastic bodies in contact", *J. Appl. Mech. – TASME*, **16**, 259-268.
- Moore, I. (1995), "Numerical modeling of blowing snow around buildings", Ph.D. Dissertation, University of Leeds, Leeds.
- Murakami, S. (2000), "Computational environment design for indoor and outdoor climates", University of Tokyo Press, Tokyo, Japan.
- Машгиз (1967), "Снегоочиститель", Москве, Россия.
- Scapozza, C. and Bartelt, P. (2003), "Triaxial tests on snow at low strain rate. Part II. Constitutive behavior", *J. Glaciology*, **49**(164), 91-101.
- Sundsbo, P.A. (1998), "Numerical simulations of wind deflection fins to control snow accumulation in building steps", *J. Wind Eng. Ind. Aerod.*, **74-76**, 543-552.
- Thiis, T.K. (2000), "A comparison of numerical simulations and full-scale measurements of snowdrifts around buildings", *Wind Struct.*, **3**(2), 73-81.
- Thiis, T.K. (2003), "Large scale studies of development of snowdrifts around buildings", *J. Wind Eng. Ind. Aerod.*, **91**(6), 829-839.
- Tominaga, Y. and Mochida, A. (1999), "CFD prediction of flowfield and snowdrift around a building complex in a snowy region", *J. Wind Eng. Ind. Aerod.*, **81**, 273-282.
- Tominaga, Y., Mochida, A. and Yoshino, H. et al. (2006), "CFD prediction of snowdrift around a cubic building model", *Proceedings of the 4th International Symposium on Computational Wind Engineering*, Yokohama, Japan, December.
- Tominaga, Y., Okaze, T. and Mochida, A. (2011), "CFD modeling of snowdrift around a building: An overview of models and evaluation of a new approach", *Build. Environ.*, **46**, 899-910.
- Tsuchiya, M., Tomabechi, T., Hongo, T. and Ueda, H. (2002), "Wind effects on snowdrift on stepped flat roofs", *J. Wind Eng. Ind. Aerod.*, **90**(12-15), 1881-1892.
- Uematsu, T., Nakata, T., Takeuchi, K. and Arisawa, Y. and Kaneda, Y. (1991), "Three-dimensional numerical simulation of snowdrift", *Cold Regions Sci. Technol.*, **20**(1), 65-73.
- Wang, W.H., Liao, H.L. and Li, M.S. (2014), "Wind tunnel test on wind-induced roof snow distribution", *J. Build. Struct.*, **35**(5), 135-141. (in Chinese)
- Yamagishi, Y., Kimura, S., Ishizawa, K., Kikuchi, M., Morikawa, H. and Kojima, T. (2012), "Visualization of snowdrift around buildings of an Antarctic base through numerical simulation", *J. Visualization*, **15**(1), 78-84.
- Zhang, Y., Li, Y., Yang, J. and Liu, D. (2011), "Statistical particle stress in aeolian sand movement-derivation and validation", *Powder Technol.*, **209**(1), 147-151.
- Zhao, T., Houlsby, G.T. and Utili, S. (2014), "Investigation of submerged debris flows via CFD-DEM coupling", *Int. Symp. on geomechanics from Micro to Macro*, Is Cambridge.
- Zhou, X.Y., Liu, C.Q., Gu, M. and Tan, M.H. (2015), "Application of Lagrangian method to snowdrift model", *J. Eng. Mech. - ASCE*, **32**(1), 36-42. (in Chinese)